International Journal of Heat and Mass Transfer 116 (2018) 694–702

Contents lists available at ScienceDirect

International Journal of Heat and Mass Transfer

journal homepage: www.elsevier.com/locate/ijhmt

An optical-thermal model for laser-excited remote phosphor with thermal quenching

Yupu Ma, Wei Lan, Bin Xie, Run Hu, Xiaobing Luo *

State Key Laboratory of Coal Combustion, School of Energy and Power Engineering, Huazhong University of Science and Technology, Wuhan 430074, China

ARTICLE INFO

Article history:
Received 26 June 2017
Received in revised form 5 September 2017
Accepted 17 September 2017

Keywords:
Remote phosphor
Phosphor modeling
Thermal quenching
Laser diode
Optical-thermal model

ABSTRACT

Laser-excited remote phosphor (LERP) has been reported to be an effective approach to produce high-luminance white light based on laser diodes (LDs). However, the local phosphor temperature may easily reach thermal quenching point due to the local high light power density, resulting in a significant drop/deterioration of efficiency, reliability and lifetime. In this paper, we focused on the phosphor thermal quenching and developed an optical-thermal coupling model to predict the high phosphor temperature of LERP. From this model, both accurate phosphor heating and temperature can be obtained by iteration. For validation, experiments were performed to verify the model and good agreement was observed between the measurements and the theoretical predictions. Based on the validated model, the critical incident power against thermal quenching under various factors was systematically studied. It was found in the experiments that when a 680 mW laser spot with a diameter of 1.0 mm was projected onto a phosphor layer, the phosphor temperature was as high as 549.0 °C, which would result in severe thermal quenching and even silicone carbonization. It was also found that increasing pump spot from 0.5 mm to 3.0 mm can dramatically enhance critical power by 19 times. The effect of decreasing phosphor layer thickness on critical power enhancement was explained by the model. Some suggestions were also provided to prevent thermal quenching and improve the optical/thermal performance of LERP.

1. Introduction

High-power phosphor-converted light-emitting diodes (pc-LEDs) have gained wide applications in general lighting [1]. However, the state-of-the-art LEDs are still suffering from the "efficiency droop", i.e. a decrease of quantum efficiency at high operating current density [2]. In contrast, laser diodes (LDs) can achieve higher efficiency at high current density, because the Auger recombination no longer grows after the threshold current [3,4]. Moreover, LDs also exhibit other excellent characteristics, including directional beam pattern and small light-emitting area, enabling the capability of high-luminance and collimated lighting [4,5]. Similar to white LEDs, pc-LDs gain more attention with their advantages of high efficiency, low cost, and compact size [6–8]. Laser-excited remote phosphor (LERP) has been commonly used in pc-LD packaging [9,10].

In LERP, light emitted from the LD chip is usually focused onto a phosphor layer, and the luminance is usually much higher than that of conventional white LEDs [11]. Consequently, the phosphor temperature will be much higher than LEDs due to the extremely higher radiant power density from LDs. High phosphor temperature will result in the severe thermal quenching problem, which will decrease the efficiency, deteriorate the reliability, and shorten the lifetime of LERP [12]. Although thermal quenching has been regarded as a significant obstacle to the development of high-luminance pc-LDs, there are quite few efficient/accurate tools/methods for evaluation. Either the phosphor temperature or the heat flux generated by the phosphors are quite hard to measure in the experiments.

Monte-Carlo ray-tracing simulations together with finite element method (FEM) have been widely used to evaluate the optical and thermal performances of pc-LEDs [13–15]. In the most methods used for phosphor modeling in pc-LEDs, the optical and thermal effects were independent of each other and this may not lead to misunderstanding because phosphor temperature is relatively low and the thermal quenching effect is not severe. But for pc-LDs, the thermal quenching is too significant to be ignored. In general, the temperature dependence of phosphor quantum efficiency was usually not considered, making it impossible to evaluate thermal quenching [16]. Actually, light scattering, absorption, conversion, and thermal quenching are interacted with each other, making it difficult and complicated for the numerical simulation. Moreover, the quantum efficiency has complex dependencies on

* Corresponding author.
E-mail address: luoxb@hust.edu.cn (X. Luo).

https://doi.org/10.1016/j.ijheatmasstransfer.2017.09.066
0017-9310/

Nomenclature

A	cross-sectional area, mm^2
A_{conv}	total convective area, mm^2
A_n, B_n	Fourier coefficients
Bi	Biot number, $hD/(2\lambda)$
c	phosphor concentration, g/cm^3
d	thickness, mm
D	diameter, mm
E_0	fitted activation energy, 6500 1/cm
$E(z)$	forward-scattering light function, W
$F(z)$	back-scattering light function, W
h	convective coefficient, W/(m^2 K)
i	ith iteration
$J_1(\cdot)$	Bessel function of first kind
k_B	Boltzmann constant
L	length, mm
P_{in}	incident laser power, W
P_{limit}	critical incident power, W
P_{out}	total output light power, W
Q_{ph}	phosphor heating power, W
R	thermal resistance, K/W
R_s	thermal spreading resistance, K/W
T_a	ambient temperature, °C
T_c	critical phosphor temperature, °C
T_{ph}	phosphor temperature, °C
W	width, mm
W_0	fitted frequency factor, 4×10^{13} 1/s
z	invasion depth, mm

Greek symbols

γ	reflection coefficient
δ_n	eigenvalues, $J_1(\delta_n) = 0$
ε	relative source size, D_{spot}/D_{ph}
ζ	relative thickness, $d_{ph}/(D_{ph}/2)$
η	phosphor quantum efficiency
λ	thermal conductivity, W/(m·K)
τ_r	radiative lifetime, s
τ_{nr}	non-radiative lifetime, s

Subscript

a	ambient
bond	bonding layer
B	blue light
conv	convection
eq	equivalent
hs	heat sink
mir	mirror layer
ph	phosphor layer
spot	laser spot
tot	total
Y	yellow light

temperature and it is hard to establish the exact relationship between them. Recently, to tackle this problem, Correia et al. proposed a method to mesh the phosphor layer using tetrahedral element discretization and stored the optical and thermal flux. Despite its complexity in meshing, this method proved to be an effective way to characterize the overall performance of pc-LED/LDs [16]. Alternatively, Lenef et al. used a diffusion-approximation radiation transport model to calculate optical effects and then coupled with FEM to study the thermal effects of pc-LDs [12,17]. In our previous papers, we have established a phosphor scattering model based on the Kubelka–Munk theory to analyze the phosphor heating effects in pc-LEDs [18,19]. We also build the thermal resistance model to predict the junction temperature of LEDs with high accuracy [20,21]. Can we apply these models to evaluate the thermal quenching directly? The answer may be NO because (1) the phosphor scattering model only considers the light-to-heat conversion part with a constant phosphor quantum efficiency (QE) and (2) the thermal resistance model only consider the heat dissipation part. Actually, the essence of thermal quenching is the temperature dependence of phosphor QE. An intuitive but feasible way is to combine our previous two models together with considering the temperature-dependent phosphor QE simultaneously.

In this paper, we attempted to develop an optical-thermal coupling model to study phosphor quenching effects on optical/thermal performance of LERP. The interacted optical and thermal effects were coupled by introducing the temperature dependence of phosphor QE. In this way, the existing phosphor model could be extended to evaluate phosphor thermal quenching effects under extremely high radiant power density of LDs. In addition, the complicated light-to-light and light-to-heat processes were simplified into a series of analytical equations and could be solved in a fast and accurate way. Optical and thermal experiments were conducted to verify the model. Based on this model, we systematically studied the effects of various factors on critical radiant power against thermal quenching. Finally, practical guidelines were provided to enhance radiant limit for high-reliability LERPs.

2. Model establishment

Fig. 1 illustrates the schematic of the optical-thermal model for LERP. A typical reflective LERP package consists of LD chip, phosphor layer, mirror layer, bonding layer, and heat sink [12,17]. The blue light and converted yellow light will be reflected on the mirror surface, and the output white light is in the opposite direction of incident light. Along with light conversion and mixing process, there is also light-to-heat conversion known as phosphor heating [22]. Due to the relatively low thermal conductivity of phosphor-silicone mixture (~0.2 W m^{-1} K^{-1}), the heat generated within the phosphor layer may not be dissipated efficiently, resulting in local high phosphor temperature and thermal quenching problem. As shown in Fig. 1, the present model consists of two sub-models, i.e. (a) phosphor scattering model and (b) steady-state thermal resistance model, and they are connected through the interaction between phosphor heating power Q_{ph} and phosphor temperature T_{ph}.

The first sub-model, i.e. phosphor scattering model, has been proposed and developed to evaluate phosphor heating for pc-LEDs [18,19,23,24]. As shown in Fig. 1(a), when the collimated laser beam is projected onto the phosphor layer, light absorption, scattering and conversion processes happen simultaneously. In this case, four light components can be derived as forward-scattering and back-scattering energy for blue and yellow light $E_B(z)$, $E_Y(z)$, $F_B(z)$ and $F_Y(z)$, respectively. Based on the energy conservation law and the modified Kubelka–Munk theory, four differential equations can be established with respect to the four light components. It should be pointed out that the boundary conditions are different from that of pc-LEDs and need to be re-expressed as follows.

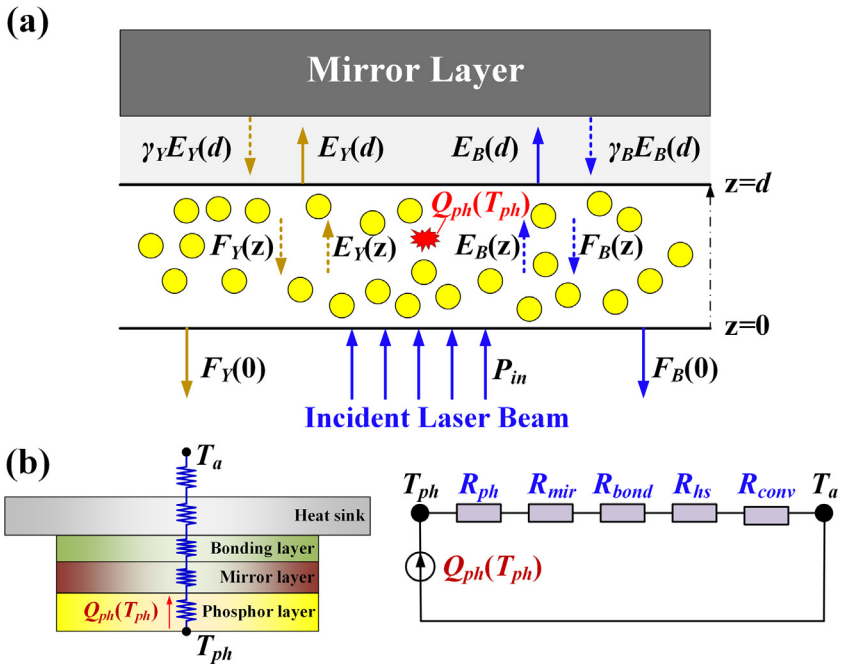

Fig. 1. Schematic of the optical-thermal model for LERP comprising (a) phosphor scattering model and (b) thermal resistance model.

For blue light:

$$E_B(0) = P_{in}, \quad F_B(d) = \gamma_B E_B(d) \tag{1}$$

For yellow light:

$$E_Y(0) = 0, \quad F_Y(d) = \gamma_Y E_Y(d) \tag{2}$$

Substituting the boundary conditions to the four differential equations, we can obtain the general forms of the four light components. More details can be found in our previous work [19]. Till then, total heat generation of phosphor layer Q_{ph} can be calculated by subtracting output optical power P_{out} from input optical power P_{in} [24]:

$$Q_{ph} = P_{in} - P_{out} \tag{3}$$

where

$$P_{out} = F_B(0) + F_Y(0) \tag{4}$$

After calculating Q_{ph}, steady-state thermal resistance model is applied to calculate phosphor temperature T_{ph}. For reflective remote phosphor, the highest concentration of converted light was found to be very close to the incident surface, i.e., z = 0 [17]. Therefore, phosphor temperature node is assumed to be located at z=0. It should be noted that the heat flow path from the incident surface to the ambient is ignored because the natural convective heat transfer is very weak with relatively small heat transfer coefficient and area. In this case, the total thermal resistance between T_{ph} and the ambient temperature T_a is composed of a series thermal resistance, as shown in Fig. 1(b), which can be expressed as:

$$R_{tot} = R_{ph} + R_{mir} + R_{bond} + R_{hs} + R_{conv} \tag{5}$$

where R_{ph}, R_{mir}, R_{bond}, and R_{hs} are conductive thermal resistance of phosphor layer, mirror layer, bonding layer, and heat sink, respectively, which can be calculated accordingly:

$$R_j = \frac{d_j}{\lambda_j A_j}, \ (j = ph,\ mir,\ bond,\ and\ hs) \tag{6}$$

and R_{conv} denotes convective thermal resistance between heat sink with the ambient:

$$R_{conv} = \frac{1}{hA_{conv}} \tag{7}$$

However, the above thermal resistances are not enough without considering thermal spreading resistance. Fig. 2 shows a circular phosphor plate with diameter of D_{ph} excited by a circular pump spot with diameter of D_{spot}. To achieve high-luminance lighting, D_{spot} is usually very small, resulting in a large ratio of D_{ph} to D_{spot}. In this case, the thermal spreading resistance from pump spot to the plate $R_{s,ph}$ plays a main role in the R_{tot} and need to be included. $R_{s,ph}$ can be calculated based on the analytical solutions for an isotropic disk with circular heat source [21,25] and the general form is:

$$R_{s,ph} = \frac{4}{\pi\varepsilon\lambda_{ph}D_{spot}}\sum_{n=1}^{\infty}A_n(n,\varepsilon)B_n(n,\zeta)\frac{J_1(\delta_n\varepsilon)}{\delta_n\varepsilon} \tag{8}$$

where

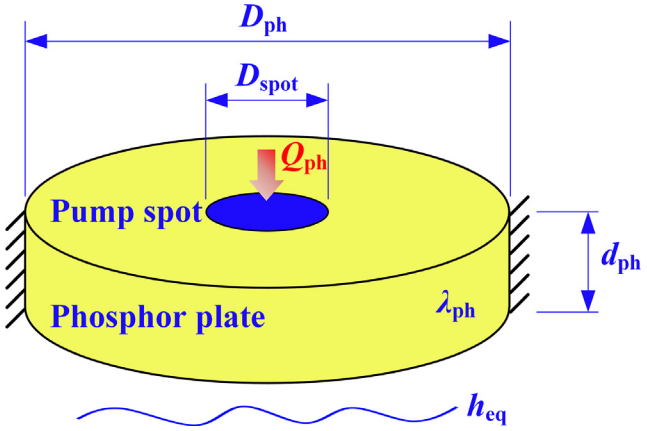

Fig. 2. Schematic of thermal spreading resistance from laser spot to a circular phosphor plate.

$$A_n = -\frac{2\varepsilon J_1(\delta_n \varepsilon)}{\delta_n^2 J_0^2(\delta_n)},\ B_n = -\frac{\delta_n + B_i \tanh(\delta_n \xi)}{\delta_n \tanh(\delta_n \xi) + B_i} \quad (9)$$

More details can be found in Refs. [21,25]. Similarly, the thermal spreading resistance from the bonding layer to the heat sink $R_{s,hs}$ can also be calculated using Eq. (8). It should be noted that Eq. (8) is also applicable for the rectangular plate after transforming the rectangular one into a circular one [21]. Finally, T_{ph} can be calculated by:

$$T_{ph} = T_a + Q_{ph}(R_{s,ph} + R_{ph} + R_{mir} + R_{bond} + R_{s,hs} + R_{hs} + R_{conv}) \quad (10)$$

After defining the phosphor scattering and thermal resistance model, the optical-thermal coupling model is constructed by further introducing the temperature dependence of phosphor QE $\eta(T_{ph})$, which can be calculated as:

$$\eta(T_{ph}) = \frac{\tau_{nr}(T_{ph})}{\tau_{nr}(T_{ph}) + \tau_r} \quad (11)$$

The temperature dependence of $\tau_{nr}(T_{ph})$ is calculated by Eq. (12) [26,27].

$$\tau_{nr}(T_{ph}) = \frac{1}{W_0} \exp\left(\frac{E_0}{k_B T_{ph}}\right) \quad (12)$$

For YAG:Ce, the fitted values for W_0 (4×10^{13} 1/s), and E_0 (6500 1/cm) are all obtained according to the literature [26]. τ_r is assumed to be a constant due to its weaker temperature dependence than τ_{nr}. We can obtain a τ_r of 67 ns for YAG:Ce from the fitting of the reported experimental curve of lifetime [26,28]. Fig. 3 shows the flowchart of the optical-thermal model. When inputting the initial T_{ph} (e.g., $T_{ph} = T_a$), we can obtain η by Eq. (11), Q_{ph} by Eq. (3) and finally an updated T_{ph} by Eq. (10) in sequence. If the updated T_{ph} does not change significantly between consecutive steps (e.g., $T_{ph}(i+1) - T_{ph}(i) < 0.01$ K), the whole framework ends and output the ultimate $T_{ph}(i+1)$. Otherwise, the iterative calculations will be continued until thermal equilibrium is reached. Through this iteration, both accurate phosphor heating and temperature can be obtained. The whole calculations were done by coding using the commercial software Matlab.

3. Experiments

Optical and thermal measurements were performed to verify the calculated P_{out} and T_{ph}, respectively. Fig. 4 shows the schematic of the (a) optical and (b) thermal test setup. A commercial LD (L450P1600MM, Thorlabs) was mounted onto a heat sink to lower the junction temperature and thus enable a stable output. The LD was driven by a current controller (LDC220C, Thorlabs). A pair of adjustable collimated and focused lenses was used to obtain collimated laser spot with a diameter of about 1 mm. A circular phosphor plate (powder phosphor embedded in silicone matrix) was glued onto an aluminum mirror with a reflectivity of 95%. Finally, the mirror was bonded with a designed phosphor plate-finned heat sink by thermal grease.

For optical test, as shown in Fig. 4(a), the whole setup was placed in an integrating sphere (ATA-1000, Everfine) and the output optical power P_{out} was measured. For thermal test, as shown in Fig. 4(b), an infrared (IR) thermal imager (SC620, FLIR) was used to capture the surface temperature of the phosphor plate. Before test, the emissivity of phosphor surface was calibrated. In the calibration process, a thermocouple was attached tightly onto the surface of phosphor layer by conductive adhesive tape. Then the phosphor layer was heated evenly by a heating plate. When it reached thermal steady state, the surface temperature was measured to be 54.1 °C. Then adjust the emissivity until the temperature of phosphor surface reached the same value. In this way, the calibrated emissivity of phosphor surface was 0.94. It should be noted that the laser beams were projected onto the plate in a small deflection angle (~10°) so that the IR can be placed normal to the phosphor target. To validate the change of P_{out} and T_{ph} with varying factors, several easy-to-implement variations were conducted. Different driving current varying from 0 A to 0.80 A with an interval of 0.05 A was used. Then three different phosphor plates were made with varying phosphor concentration of 0.11 g/cm^3, 0.22 g/cm^3, and 0.32 g/cm^3, respectively. The thermal conductivities and geometric parameters of the components involved in the model were listed in Table 1.

4. Model validation by experiments

For validation, P_{out} and T_{ph} need to be calculated using the presented model. Besides the parameters listed in Table 1, additional inputs should be obtained according to the experimental configuration. The absorption and scattering coefficient of phosphor particles toward blue and yellow light were calculated based on the Mie–Lorenz theory [29]. The peak wavelength of blue and converted yellow light were measured to be 447 nm and 558 nm, respectively, corresponding to a Stokes shift efficiency of ~0.80.

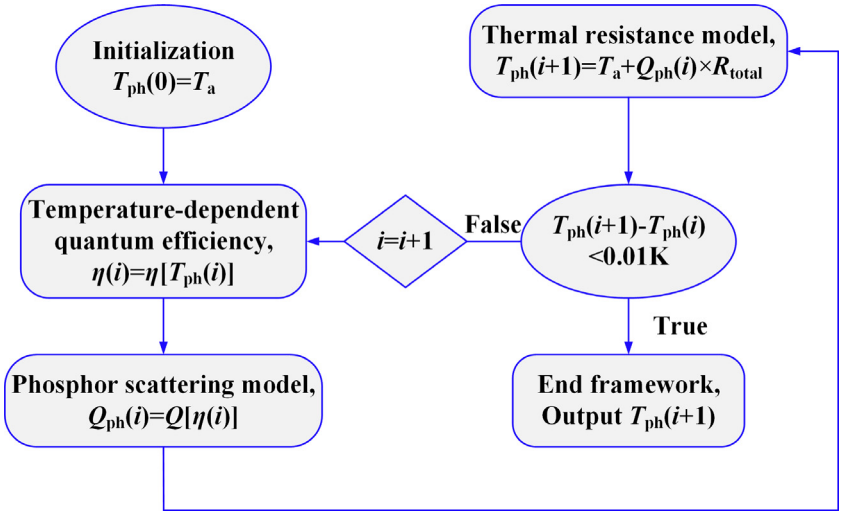

Fig. 3. Flowchart of the optical-thermal model considering thermal quenching effects.

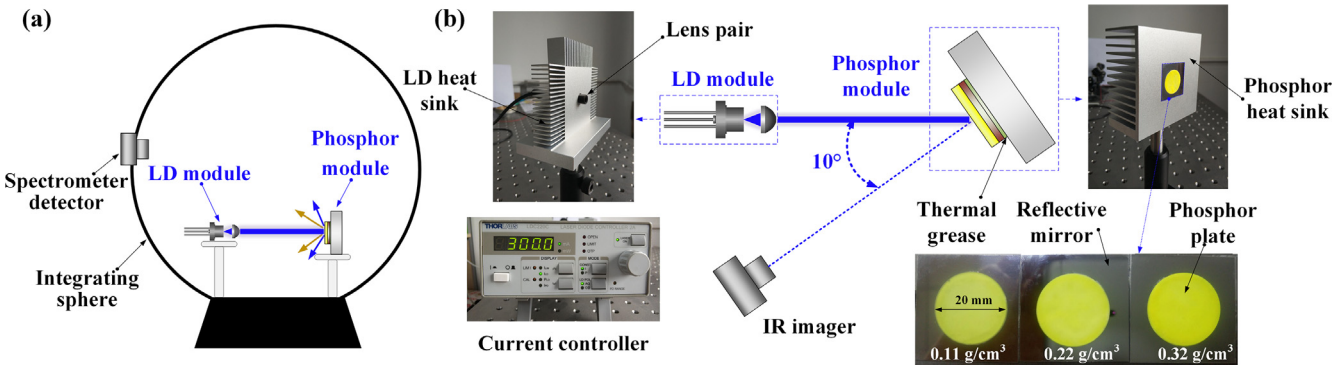

Fig. 4. The schematic of the (a) optical and (b) thermal test setup.

Table 1
The thermal conductivities and geometric parameters of the components.

Components	Materials	Thermal Conductivity (W tm^{-1} K^{-1})	Thickness (mm)	Cross-sectional dimensions (mm)
Phosphor plate	phosphor/silicone	0.17	0.32	$D = 20$
Reflective mirror	Al 7075-T6	130	0.45	$W \times L = 30 \times 30$
Thermal grease	/	0.67	0.1	$W \times L = 30 \times 30$
Phosphor heat sink	Al 6061-T6	167	/	$W \times L = 80 \times 80$

The natural convective coefficient h was calculated to be 0.52 W/(m^2 K) based on the empirical equations for the designed rectangle fin arrays [30].

Fig. 5 shows the measured IR images under 0.11 g/cm^3 and varying current of 0.25 A and 0.8 A, respectively. We can see that the maximum temperature is located at the center of the spot and regarded as the measured T_{ph}. When the current rises from 0.25 A to 0.8 A, T_{ph} shows a great increase from 48.9 °C to 549.0 °C, resulting in thermal quenching and even silicone carbonization, which corresponds to the central blackening point as shown in Fig. 6(b). A similar phenomenon was also observed in pc-LED array under total input electrical power of 31 W in our previous study [22].

In order to further understand the phenomenon and verify our model, the measured results versus different currents and concentrations are analyzed. Fig. 7(a) shows the output power and voltage of LD versus varying current from 0 A to 0.80 A with an interval of 0.05 A. We can see that the LD threshold current is about 0.20 A and P_{in} rises approximately linearly with the current above threshold. Fig. 7(b–d) demonstrate the comparisons between the measured and calculated T_{ph} and P_{out} versus P_{in} under varying phosphor concentration of 0.11 g/cm^3, 0.22 g/cm^3, and 0.32 g/cm^3, respectively. Similar trends can be observed among them. We can see from Fig. 7(b) that both the measured P_{out} and T_{ph} first increase with T_{in}, which can be easily understood by the increased input power and phosphor heat generation, respectively. However, sudden changes happen when P_{in} exceeds a critical value. With P_{in} varying from 650 mW to 680 mW, T_{ph} shows a rapid rise from 198.0 °C to 549.0 °C, corresponding to a sudden drop of P_{out} from 473 mW to 243 mW. This observation can be explained by the temperature-dependent $\eta(T_{ph})$. Fig. 8 plots the normalized QE versus T_{ph} obtained by Eq. (11). When T_{ph} is approaching the onset quenching temperature T_c (i.e., $T_{0.95}$ corresponding to 95% of the peak QE shown in Fig. 8) [31], the decrease of η leads to a rise of Q_{ph} and T_{ph}, and conversely results in a decline in η [17]. This thermal runaway effect finally leads to a higher T_{ph} far exceeding quenching temperature $T_{0.5}$ corresponding to 50% of the peak QE [31], demonstrating the occurrence of the thermal quenching.

It can also be observed that under low P_{in}, the experimental results agree well with the calculations. However, the deviation can be large as P_{in} grows. We obtained that when P_{in} reaches 630 mW, the maximum difference between the measured and calculated P_{out} and T_{ph} are 48.7 mW and 21.5 °C, with corresponding errors of 10.1% and 9.7%, respectively. The deviations are within

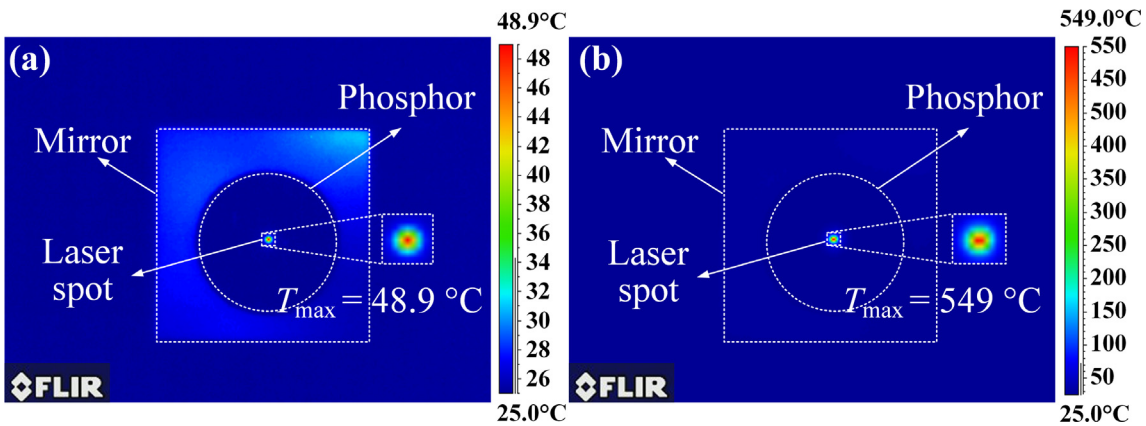

Fig. 5. The measured IR images and the enlarged central spot (in the right rectangle) under 0.11 g/cm^3 and varying current of (a) 0.25 A, (b) 0.8 A, respectively.

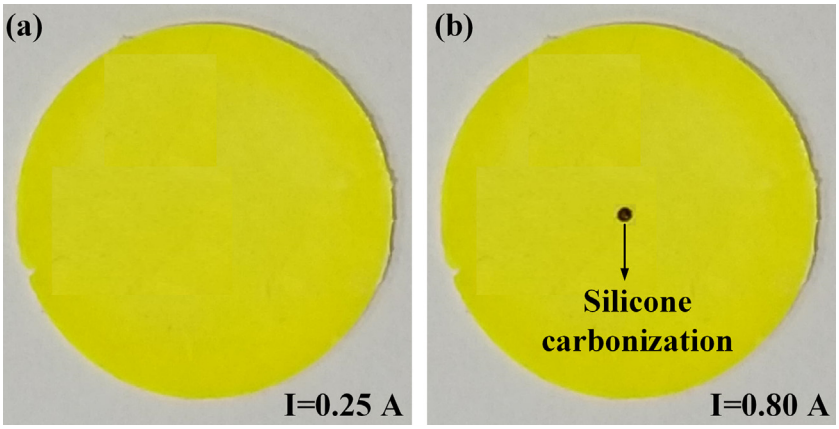

Fig. 6. The photographs of phosphor plate under current of (a) 0.25 A and (b) 0.80 A, respectively.

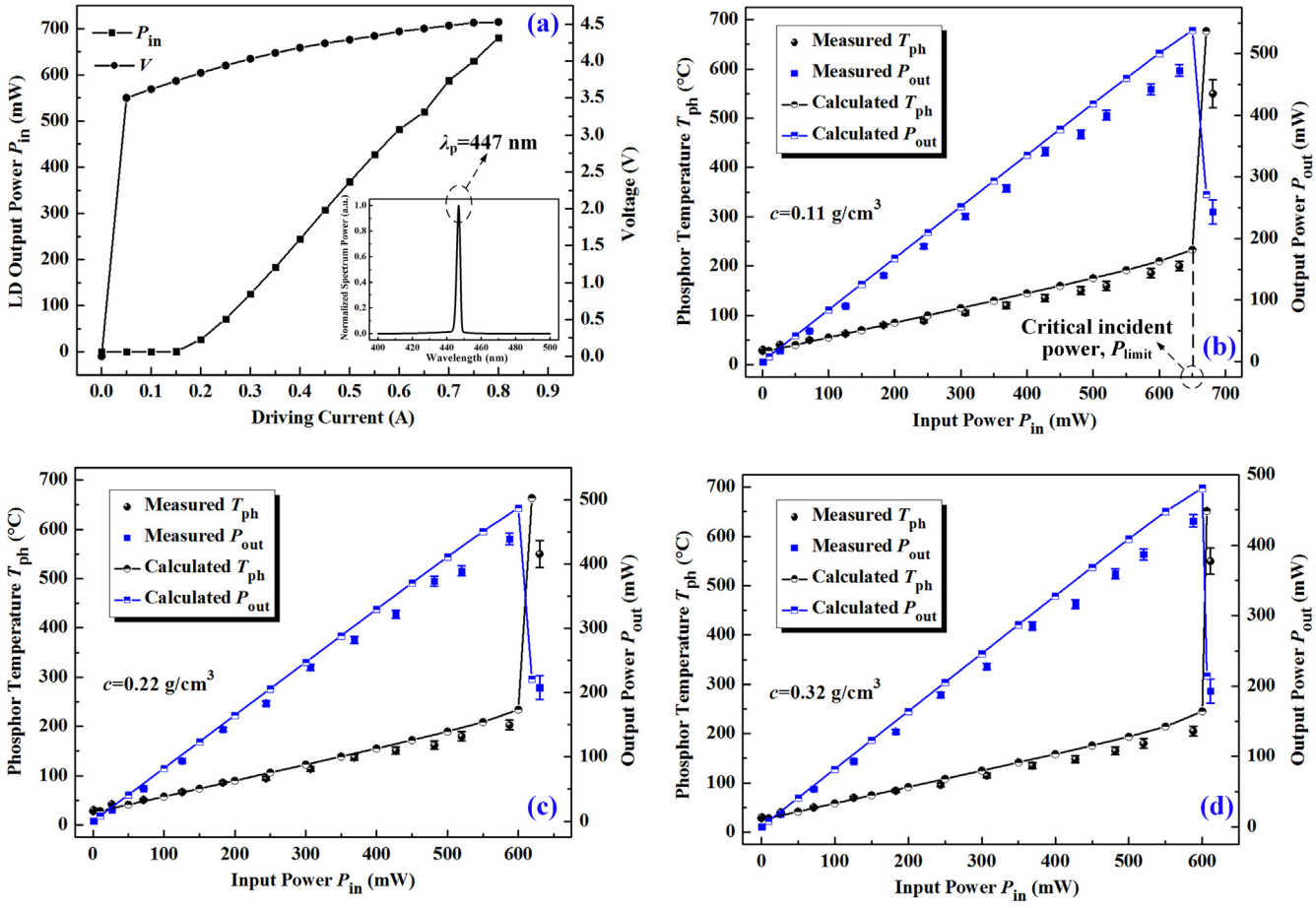

Fig. 7. (a) The measured P-I-V curves of LD (the inset is the normalized spectrum power distribution of LD); and the comparison between the calculated and measured T_{ph} and P_{out} under varying phosphor concentration of (b) 0.11 g/cm^3, (c) 0.22 g/cm^3, and (d) 0.32 g/cm^3, respectively.

an acceptable range, especially in view of the same trends shared by the measurements and calculations. In addition, the measured P_{out} is always lower than the calculated one because part of output light is absorbed by the whole setup due to reflection loss, resulting in a decrease of P_{out}. It should also be mentioned that, when thermal quenching occurs, the T_{ph} of test (549.0 °C) is obviously lower than calculation (677.1 °C) because of the limitation of the IR imager. Moreover, in actual, the rapid increase of T_{ph} can occur quite quickly on millisecond time-scales, making it hard to probe the accurate phosphor temperature. In this case, the absolute value doesn't make much sense as long as thermal quenching occurs. Hence, this large deviation may not affect the feasibility of the model in evaluating thermal quenching effects.

5. Parameter analysis on P_{limit}

In order to characterize and analyze the thermal quenching effects, we defined the input power corresponding to the turning point shown in Fig.7(b) as the critical incident power P_{limit}. It can be seen that only a few tens of milliwatts above P_{limit} can lead to

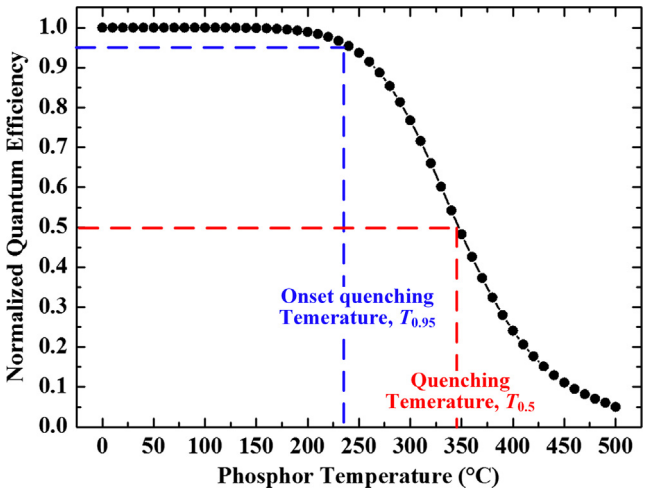

Fig. 8. The normalized phosphor quantum efficiency versus phosphor temperature of YAG:Ce.

thermal quenching. Obviously, for a given laser spot, the highest attainable output power and radiance are both limited by P_{limit}. Hence, it is vital to investigate the methods to enhance P_{limit}, and thus alleviate thermal quenching. For better understanding, P_{limit} can be approximately expressed as follows by transforming Eq. (10):

$$P_{limit} = \frac{T_c - T_a}{Q_{ph}/P_{in}R_{tot}} \tag{13}$$

For a given type of phosphor, the critical temperature T_c can be regarded as a fixed value. Hence, P_{limit} is inversely proportional to the product of Q_{ph}/P_{in} and R_{tot}. In the following, using the model, we conducted overall parameter analysis on P_{limit}. The involving parameters can be divided into optical, thermal and optical-thermal factors. This classification is based on whether Q_{ph}/P_{in} or R_{tot} is mainly affected.

Fig. 9 illustrates effects of optical factors on P_{limit}, including phosphor concentration c and mirror reflectivity γ ($\gamma_B = \gamma_Y$). One can observe that a rise of P_{limit} can be achieved by decreasing c or increasing γ. And the strong dependence is seen in the low concentration or high reflectivity region. When γ rises from 0.8 to 1.0, P_{limit} can be increased by 2.1 times. A similar observation was reported in Ref. [17]. The developing trend of P_{limit} can be understood, based on Eq. (13), by the opposite variation of Q_{ph}/P_{in}, with R_{tot} remaining a constant. Another key parameter to characterize phosphor heating is the quantum efficiency. It is apparent that strengthening thermal stability, i.e., increasing onset quenching temperature T_c, can also dramatically enhance P_{limit}. Previous researches have reported that the single-crystal phosphor can withstand higher radiance compared with conventional powder phosphor, contributing to high luminance [6,32].

Fig. 10 shows effects of thermal factors on P_{limit}, including pump spot diameter D_{spot} and convective coefficient h. It should be noted that other thermal parameters, e.g. the thermal conductivity and thickness of mirror and bonding layer, are not discussed because of the corresponding relative small thermal resistance in the simulated case. It is seen that P_{limit} rises with both increasing D_{spot} and h, which can also be easily explained by the changing R_{tot}, with Q_{ph}/P_{in} unchanged. Substantial enhancement of P_{limit} versus D_{spot} is also found, e.g. when D_{spot} increases from 0.5 mm to 3.0 mm, P_{limit} can be enhanced by 19 times. It is because that $R_{s,ph}$ dominates R_{tot} and small change in D_{spot} can result in large difference of $R_{s,ph}$. But increasing spot size may weaken the luminance [17], so there is a trade-off and this problem is worth further research. On the other hand, P_{limit} may not rise with h under high h, implying that there may exist limitation in increasing P_{limit} by enhancing convective heat transfer.

Fig. 11 demonstrates the effect of optical-thermal factor on P_{limit}. As shown in Fig.11(b), with varying phosphor layer thickness d_{ph}, both Q_{ph}/P_{in} and R_{tot} change. When d_{ph} increases, R_{tot} drops due to decreased $R_{s,ph}$ [21], but Q_{ph}/P_{in} rises instead due to more absorbed light [22]. The combined effect leads to a first sudden and then slight increase of the product of them (shown in the inset figure), corresponding to the opposite trend of P_{limit} versus d_{ph} shown in Fig.11(a). This implies that Q_{ph}/P_{in} plays a dominant role, especially in low d_{ph} region. So thinner phosphor layer is preferable in terms of small phosphor heating, but the reduced yellow to blue light ratio may be a concern [1].

In summary, simultaneous lower phosphor heating and total thermal resistance are preferred to enhance P_{limit}, and finally improve the optical-thermal performance of LERPs. This may be achieved by combining two or more methods presented above.

6. Conclusions

In this paper, we presented an analytical optical-thermal model, coupling phosphor scattering model with steady-state thermal resistance model, to evaluate the thermal quenching effects of laser-excited remote phosphor by further considering the temperature dependence of phosphor quantum efficiency. To validate the

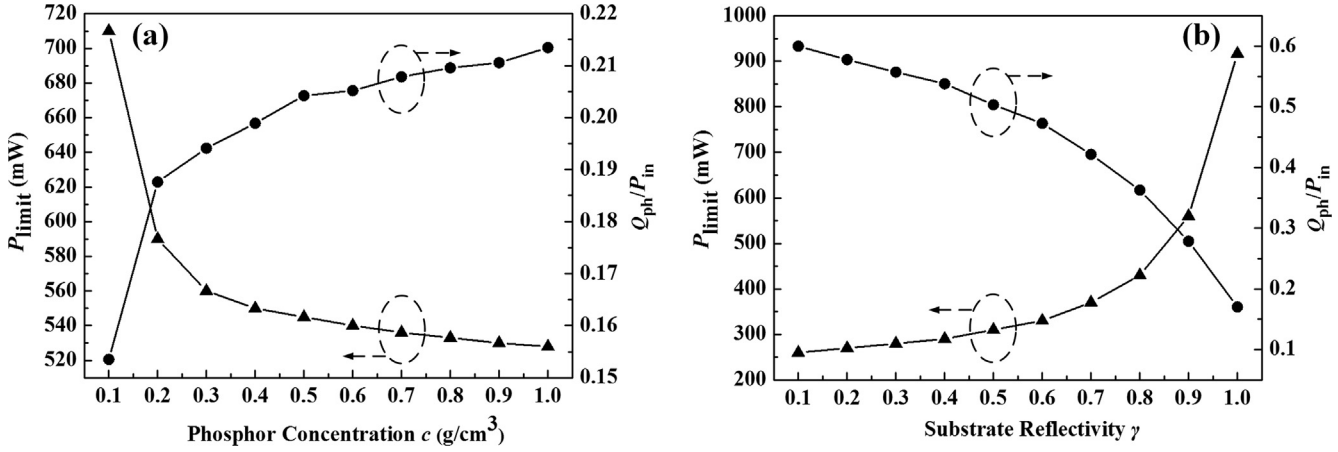

Fig. 9. Effects of optical factors on P_{limit}: (a) phosphor concentration c and (b) mirror reflectivity γ.

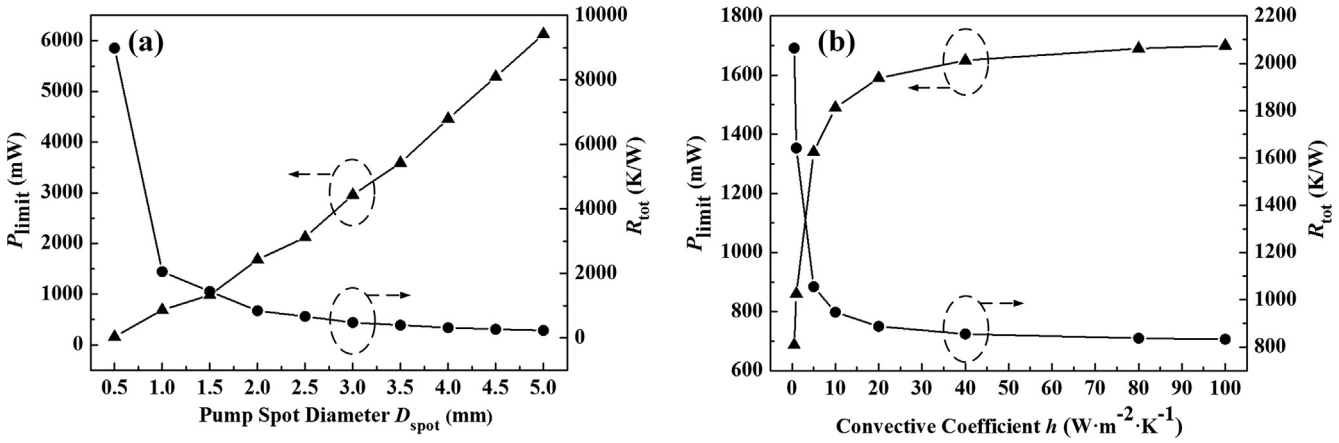

Fig. 10. Effects of thermal factors on P_{limit}: (a) pump spot diameter D_{spot} and (b) convective coefficient h.

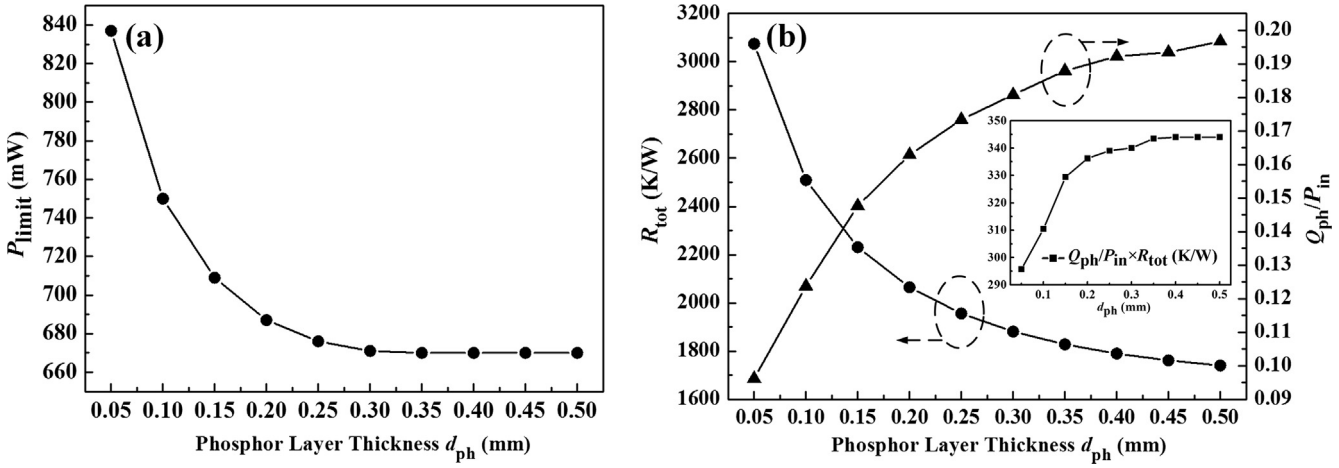

Fig. 11. (a) The effect of optical-thermal factor phosphor layer thickness d_{ph} and (b) the corresponding mechanism.

model, optical and IR measurements were conducted and the measured and calculated P_{out} and T_{ph} agreed well with each other, with the corresponding maximum deviation of 10.1% and 9.7%, respectively. Critical incident power P_{limit} was observed, only a few tens of milliwatts above which thermal quenching occurred immediately. It was attributed to the interplay between the increased phosphor heating and reduced quantum efficiency. For application, we systematically analyzed the effects of optical and thermal parameters on P_{limit} based on the model. We found that increasing spot diameter was the most effective method to improve P_{limit}, however, lower luminance was accompanied. This trade-off between thermal stability and luminance need to be studied in the future work. In addition, highly reflective mirror also plays a key role in critical power enhancement to relieve thermal quenching and promote better optical/thermal performance of LERP.

Acknowledgement

The authors would like to acknowledge the financial support by National Natural Science Foundation of China (51625601, 51576078, and 51606074) and by the Fundamental Research Funds for the Central Universities (2016JCTD112).

Conflict of interest

There are no conflicts of interest.

References

[1] X.B. Luo, R. Hu, S. Liu, K. Wang, Heat and fluid flow in high-power LED packaging and applications, Prog. Energy Combus. Sci. 56 (2016) 1–32.
[2] M.A.D. Maur, A. Pecchia, G. Penazzi, W. Rodrigues, A.D. Carlo, Efficiency drop in green InGaN/GaN light emitting diodes: the role of random alloy fluctuations, Phys. Rev. Lett. 116 (2) (2016) 027401.
[3] J.J. Wierer, J.Y. Tsao, D.S. Sizov, Comparison between blue lasers and light-emitting diodes for future solid-state lighting, Laser Photonics Rev. 7 (6) (2013) 963–993.
[4] J.J. Wierer, J.Y. Tsao, Advantages of III-nitride laser diodes in solid-state lighting, Phys. Status Solidi A 212 (5) (2015) 980–985.
[5] C. Basu, M. Meinhardt-Wollweber, B. Roth, Lighting with laser diodes, Adv. Opt. Technol. 2 (4) (2013) 313–321.
[6] M. Cantore, N. Pfaff, R.M. Farrell, J.S. Speck, S. Nakamura, S.P. DenBaars, High luminous flux from single crystal phosphor-converted laser-based white lighting system, Opt. Exp. 24 (2) (2015) A215.
[7] Y. Xu, L.H. Chen, Y.Z. Li, G.F. Song, Y.P. Wang, W.D. Zhuang, Z. Long, Phosphor-conversion white light using InGaN ultraviolet laser diode, Appl. Phys. Lett. 92 (2) (2008) 021129.
[8] A.F. George, S. Al-Waisawy, J.T. Wright, W.M. Jadwisienczak, F. Rahman, Laser-driven phosphor-converted white light source for solid-state illumination, Appl. Opt. 55 (8) (2016) 1899–1905.
[9] K.A. Denault, M. Cantore, S. Nakamura, S.P. DenBaars, R. Seshadri, Efficient and stable laser-driven white lighting, AIP Adv. 3 (7) (2013) 072107.
[10] D.H. Lee, J. Joo, S. Lee, Modeling of reflection-type laser-driven white lighting considering phosphor particles and surface topography, Opt. Exp. 23 (15) (2015) 18872–18887.
[11] S. Masui, T. Yamamoto, S. Nagahama, A white light source excited by laser diodes, Electron. Commun. Jpn. 98 (5) (2015) 23–27.
[12] A. Lenef, J. Kelso, Y. Zheng, M. Tchoul, Radiance limits of ceramic phosphors under high excitation fluxes, Proc. SPIE 8841 (2013) 884107–884120.
[13] P. Fulmek, C. Sommer, P. Hartmann, P. Pachler, H. Hoschopf, G. Langer, J. Nicolics, F.P. Wenzl, On the thermal load of the color-conversion elements in

phosphor-based white light-emitting diodes, Adv. Opt. Mater. 1 (10) (2013) 753–762.
[14] R. Hu, X. Luo, H. Zheng, Hotspot location shift in the high-power phosphor-converted white light-emitting diode packages, Jpn. J. Appl. Phys. 51 (2012) 09MK05.
[15] B.J. Shih, S.C. Chiou, Y.H. Hsieh, C.C. Sun, T.H. Yang, S.Y. Chen, T.Y. Chung, Study of temperature distributions in pc-WLEDs with different phosphor packages, Opt. Exp. 23 (26) (2015) 33861–33869.
[16] A. Correia, P. Hanselaer, Y. Meuret, An efficient optothermal simulation framework for optimization of high-luminance white light sources, IEEE Photonics J. 8 (4) (2016) 1601215.
[17] A. Lenef, J. Kelso, M. Tchoul, O. Mehl, J. Sorg, Y. Zheng, Laser-activated remote phosphor conversion with ceramic phosphors, in: Proc. SPIE 9190, 2014, 91900C.
[18] R. Hu, H. Zheng, J.Y. Hu, X.B. Luo, Comprehensive study on the transmitted and reflected light through the phosphor layer in light-emitting diode packages, J. Disp. Technol. 9 (6) (2013) 447–452.
[19] X.B. Luo, R. Hu, Calculation of the phosphor heat generation in phosphor-converted light-emitting diodes, Int. J. Heat Mass Tranf. 75 (2014) 213–217.
[20] Y.P. Ma, R. Hu, X.J. Yu, W.C. Shu, X.B. Luo, A modified bidirectional thermal resistance model for junction and phosphor temperature estimation in phosphor-converted light-emitting diodes, Int. J. Heat Mass Transf. 106 (2017) 1–6.
[21] X.B. Luo, Z.M. Mao, J. Yang, S. Liu, Engineering method for predicting junction temperatures of high-power light-emitting diodes, IET Optoelectron. 6 (5) (2012) 230–236.
[22] X.B. Luo, X. Fu, F. Chen, H. Zheng, Phosphor self-heating in phosphor converted light emitting diode packaging, Int. J Heat Mass Transf. 58 (2013) 276–281.
[23] D.Y. Kang, E. Wu, D.M. Wang, Modeling white light-emitting diodes with phosphor layers, Appl. Phys. Lett. 89 (23) (2006) 231102.
[24] M. Huang, L.Y. Yang, Heat generation by the phosphor layer of high-power white LED emitters, IEEE Photonics Technol. Lett. 25 (14) (2013) 1317–1320.
[25] Y.S. Muzychka, M.M. Yovanovich, J.R. Culham, Spreading thermal resistances in rectangular flux channels part I -geometric equivalences, in: Proc. 36th AIAA Thermophysics Conf. AIAA, 2003, pp. 4187.
[26] L.J. Lyu, D.S. Hamilton, Radiative and nonradiative relaxation measurements in Ce^{3+} doped crystals, J. Lumin. 48 (1991) 251–254.
[27] V. Bachmann, C. Ronda, A. Meijerink, Temperature quenching of yellow Ce^{3+} luminescence in YAG:Ce, Chem. Mater. 21 (10) (2009) 2077–2084.
[28] S. Arjoca, E.G. Víllora, D. Inomata, K. Aoki, Y. Sugahara, K. Shimamura, Temperature dependence of Ce:YAG single-crystal phosphors for high-brightness white LEDs/LDs, Mater. Res. Exp. 2 (5) (2015) 055503.
[29] Z.Y. Liu, S. Liu, K. Wang, X.B. Luo, Measurement and numerical studies of optical properties of YAG: Ce phosphor for white LED packaging, Appl. Opt. 49 (2010) 247–257.
[30] F. Harahap, H.N. McManus, Natural convection heat transfer from horizontal rectangular fin arrays, J. Heat Trans-T ASME 89 (1) (1967) 32–38.
[31] J. Ueda, P. Dorenbos, A.J.J. Bos, A. Meijerink, S. Tanabe, Insight into the thermal quenching mechanism for $Y_3Al_5O_{12}:Ce^{3+}$ through thermoluminescence excitation spectroscopy, J. Phys. Chem. C 119 (44) (2015) 25003–25008.
[32] E.G. Víllora, S. Arjoca, D. Inomata, K. Shimamura, Single-crystal phosphors for high-brightness white LEDs/LDs, in: Proc. SPIE 9768, 2016, 976805.